Intermolecular structure of liquid deuterium: A new neutron diffraction investigation

1995 J. Phys.: Condens. Matter 7 5777

(http://iopscience.iop.org/0953-8984/7/29/006)

J. Phys.: Condens. Matter 7 (1995) 5777–5791. Printed in the UK

Intermolecular structure of liquid deuterium: a new neutron diffraction investigation

Eleonora Guarini†, Fabrizio Barocchi†, Renato Magli‡, Ubaldo Bafile§ and Marie-Claire Bellissent-Funel‖

† Dipartimento di Fisica, Università di Firenze, largo E Fermi 2, I-50125 Firenze, Italy
‡ Dipartimento di Energetica, Università di Firenze, via di S Marta 3, I-50139 Firenze, Italy
§ Istituto di Elettronica Quantistica, Consiglio Nazionale delle Ricerche, via Panciatichi 56/30, I-50127 Firenze, Italy
‖ Laboratoire Léon Brillouin¶, CEN Saclay, 91191 Gif-sur-Yvette Cédex, France

Received 3 April 1995, in final form 10 May 1995

Abstract. The static centre of mass structure factor of liquid deuterium, already determined by means of time of flight neutron diffraction (as reported in *Physical Review* E in 1993), has been re-investigated with a two-axis diffractometer at a reactor source. A detailed analysis of the data is presented, with special attention devoted to the correction for inelastic scattering effects. The comparison of the two sets of data reveals the presence of discrepancies, which cannot be attributed to statistical inaccuracies. The density and the temperature derivatives of the structure factor have also been measured with high accuracy. For these quantities, the two experiments are in good agreement with each other. This suggests that the discrepancy in the structure factor is due to systematic effects which vanish in a differential measurement.

1. Introduction

The investigation of the microscopic structural properties of quantum liquids has been the subject of much experimental work, most of which has been devoted to the neutron diffraction study of helium [1]. No less important, either in principle or from an applicative point of view, would be the determination of the microscopic structure of the liquid hydrogens, particularly in the vicinity of the liquid–solid transition, where it is possible, by varying pressure and temperature within limited ranges, to obtain the same density in the liquid and in the solid phase, and to study the structural changes which occur across the melting transition.

As far as neutron diffraction is concerned, two serious experimental difficulties have made it so far impossible to study the structure of molecular hydrogen in the condensed phase. A first problem is the large ratio of the incoherent to the coherent bound atom scattering cross-section of the hydrogen nucleus, which makes the intramolecular scattering dominate over the purely coherent part which contains the intermolecular structural information. Since deuterium has a much smaller incoherent cross-section and a larger coherent one than the lighter isotope hydrogen, the D_2 molecule is a much better sample than H_2 for a neutron diffraction determination of the static structure factor.

The second problem with H_2 is that, due to the small mass of the molecule, a large amount of inelastic scattering affects the diffraction pattern and renders the extraction of

¶ Laboratoire Commun CEA–CNRS.

0953-8984/95/295777+15$19.50

the static structure factor more difficult. It is well known, in fact, that in a neutron diffraction experiment the data are interpreted within the static approximation while the inelastic scattering events are treated as an effect to be corrected for.

The experimental research, which has started only recently, has therefore concentrated on the structural properties of D_2, although it would be desirable to be able to investigate to what extent the different amount of quantum effects gives rise to differences in the structure of the two fluids. Due to the larger mass, the inelastic effects in D_2 are smaller, but still important. A previous comparison [2] of two time of flight (TOF) diffraction experiments on deuterium close to the critical point [3, 4] showed that a possible explanation of the discrepancies found at low momentum transfer Q could be found in an inadequate correction for inelastic scattering, since the data of [4] were taken in a wide range of the scattering angle θ. In fact, inelastic scattering increases with increasing θ and, in a TOF measurement, contributes mainly at low Q [5, 6].

For the liquid phase of deuterium, apart from the already mentioned measurements of [4], only one other experiment has been so far reported in the literature [6], which was carried out at the small angle neutron diffractometer for amorphous and liquid samples (SANDALS) at the ISIS pulsed source (Rutherford Appleton Laboratory, UK), where the maximum scattering angle is limited to 20.1°, and the effect of inelastic scattering is therefore reduced.

The intensity of inelastic scattering could be exactly calculated if the dynamic structure factor $S(Q, \omega)$ were known, but in that case the static structure factor could be simply obtained as $S(Q) = \int_{-\infty}^{+\infty} d\omega\ S(Q, \omega)$. However, neutron inelastic scattering spectra do not allow a determination of $S(Q)$ as accurate as obtained with the diffraction technique, although in this case the unknown dynamics can only be taken into account approximately by using model functions for $S(Q, \omega)$. A common choice is to model the atomic motions as those of an ideal gas, whose $S(Q, \omega)$ has the advantage of having the correct quantum (detailed balance) asymmetry and of not requiring the knowledge of the transport properties of the fluid.

For a molecular system, besides the correlations of the centre of mass motions (intermolecular dynamics), the presence of internal degrees of freedom must also be taken into account. In general, the molecular structure results in a great complication, since it leads to anisotropic interactions and, as a consequence, to the onset of orientational correlations. Moreover, in the case of heavy or complex molecules the effect of the rotational motions can be taken into account only in approximate ways, for instance by introducing the concept of effective mass [7]. In H_2 and D_2 the anisotropic components of the intermolecular potential are very small, therefore these systems can be considered to a very good approximation as composed of freely rotovibrating molecules even in the solid phase, provided the pressure is not too high [8]. Then it can be shown [9] that the scattering of neutrons from a system of light homonuclear diatomic molecules can be well described by assuming the free rigid-rotor approximation for the molecule, if the centre of mass dynamic structure factor $S(Q, \omega)$ is known. This theory, which takes into account exactly the quantum nature of rotations, including the effect of the nuclear spin on the symmetry of rotational states, can be generalized to a freely rotating harmonic oscillator [10, 11], and is particularly suitable for liquid H_2 and D_2.

Thus, by retaining the simple ideal gas dynamics for the centres of mass, the calculation of inelastic effects in deuterium is in principle possible. In the TOF case, however, such a calculation is difficult because the high-energy neutrons present in the beam can excite many rotational and vibrational transitions, each of them contributing to the scattering cross-section. For example, at $\theta = 10°$, in order to explore the region $Q \leqslant 70\ nm^{-1}$, where the

intermolecular correlations of D_2 are present, an incident energy up to 3.34 eV is required, while the rotational constant of deuterium is only 3.71 meV and the vibration quantum is 371.2 meV. In [6], the inelastic scattering was calculated for a monatomic ideal gas having the same total scattering cross-section as the D_2 molecule, and it turned out to contribute appreciably for $Q \leqslant 10\ \mathrm{nm}^{-1}$ only. By taking the calculation as an estimate of the inelastic scattering in D_2, it was decided to avoid performing the correction.

If neutron diffraction is carried out on a two-axis diffractometer using the monochromatic beam of a reactor source, the inelastic scattering is known to affect mainly the high-Q region, where it results in the typical decrease of the scattered intensity with increasing Q. In this case a wide θ range is necessary to obtain the Q values of interest, and the inelastic correction for a light system can thus be very large at high Q (see for example figure 1). On the other hand, the calculation of the scattering cross-section based on the diatomic ideal gas model can be carried out with better accuracy than in the TOF case, since a smaller number of rotational transitions of D_2 can be excited with the typical energy of thermal neutrons. Moreover, the larger Q is, the better the ideal gas limit approximates the centre of mass dynamics of a real system.

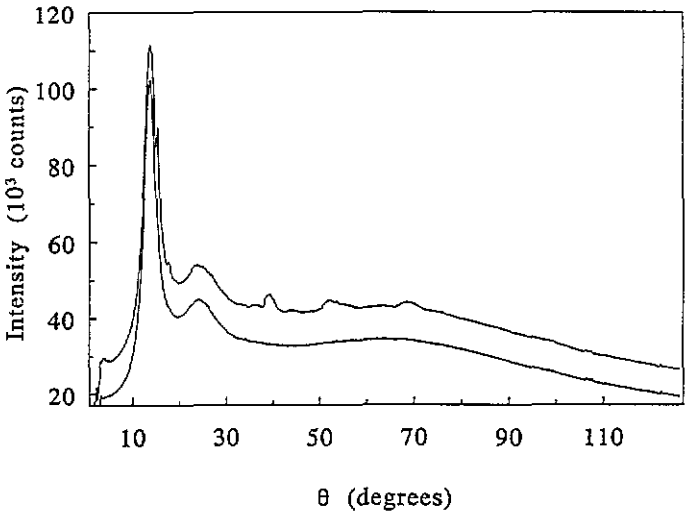

Figure 1. Effect of subtracting the container scattering for state 1: the upper curve is I_{D_2}, the lower one is $I_{D_2} - I_{He}$. The decrease of intensity due to the inelastic scattering appears clearly at high scattering angles.

We have therefore measured the static structure of liquid D_2 using a reactor-based neutron diffractometer and carefully evaluating the inelastic scattering correction. This also allows us to compare the results with those obtained with the TOF technique [6]. This paper contains a detailed description of the experiment and of the data analysis [12], and it is organized as follows. Section 2 summarizes the relevant formulae for neutron scattering from a molecular sample. In section 3 the details of the experiment are reported. Section 4 contains a description of the data analysis, divided into various subsections. In particular, we have inserted here a very detailed description of the procedure used for the absolute normalization of the data and for the correction of inelastic scattering, because we believe that this is the most accurate method available for this kind of sample. The results are presented in section 5 and compared with the TOF data of [6], while section 6 is devoted to the conclusions.

2. Theory

The double differential cross-section per molecule for the scattering of neutrons from a system of N identical homonuclear diatomic molecules can be written exactly if the orientational correlations are negligible, so that the translational dynamics is not correlated to the rotational motions, and there is only one isotopic species. For liquid D_2 both assumptions are valid and one has [9–11]

$$\frac{d^2\sigma}{d\Omega\, d\omega}(\theta,\omega) = \frac{k_1}{k_0}\frac{1}{2\pi}\int_{-\infty}^{\infty} dt \exp(-i\omega t)[F_s(Q,t)v(Q,t) + F_d(Q,t)u(Q)]$$
$$= \frac{k_1}{k_0}\tilde{S}(Q,\omega). \tag{1}$$

Here $k_0 = |k_0|$, $k_1 = |k_1|$ where k_0 and k_1 are the incident and scattered wavevectors, $Q = k_0 - k_1$ and ω are the momentum and energy transfers in units of the Planck constant $\hbar$, related by ($Q = |Q|$)

$$Q^2 = k_0^2\left[2 - \frac{\hbar\omega}{E_0} - 2\left(1 - \frac{\hbar\omega}{E_0}\right)^{1/2}\cos\theta\right]. \tag{2}$$

$E_0 = \hbar^2 k_0^2/2m$ is the incident energy, m is the neutron mass, $u(Q)$ is the intermolecular cross-section, $v(Q,t)$ is an intramolecular time-dependent form factor [9, 11], and F_s and F_d are the *self* ($p = q$) and the *distinct* ($p \neq q$) part, respectively, of the time correlation function

$$F(Q,t) = \frac{1}{N}\sum_{p,q=1}^{N}\left\langle \exp[-iQ\cdot R_p(0)]\exp[iQ\cdot R_q(t)]\right\rangle \tag{3}$$

where $R_p(t)$ is the position of the centre of mass of the pth molecule at time t in the Heisenberg representation. In (1) we have used the symbol $\tilde{S}(Q,\omega)$ to distinguish it from the centre of mass dynamic structure factor $S(Q,\omega) = S_s(Q,\omega) + S_d(Q,\omega)$, where S_s and S_d are the time Fourier transforms of F_s and F_d, respectively. Note that $S(Q,\omega)$ has the dimensions of an inverse frequency while $\tilde{S}(Q,\omega)$ has the dimensions of inverse frequency times cross-section. The centre of mass static structure factor $S(Q)$ is, by definition, the value of F at $t = 0$. Thus, using $F_s(Q,0) = 1$, one obtains $F_d(Q,0) = S(Q)$ and from equation (1)

$$\tilde{S}(Q) \equiv \int_{-\infty}^{+\infty} d\omega\, \tilde{S}(Q,\omega) = \int_{\substack{-\infty \\ Q=const}}^{+\infty} d\omega \frac{k_0}{k_1}\frac{d^2\sigma}{d\Omega\, d\omega}(\theta,\omega) = v(Q) + u(Q)[S(Q) - 1] \tag{4}$$

where we have introduced the intramolecular cross-section $v(Q) = v(Q,0)$.

3. The experiment

The experiment has been carried out on the 7C2 two-axis diffractometer at the Orphée reactor of the Laboratoire Léon Brillouin (Saclay, France), using an incident neutron wavelength $\lambda = 0.071$ nm. The scattered neutrons were collected by the position- sensitive BF_3-filled one-dimensional 'banana' detector of 7C2 in the scattering angle range $\theta \leqslant 126.1°$ with $\Delta\theta = 0.2°$.

The sample was liquid D_2 at seven thermodynamic states with densities close to that of the triple point, chosen in such a way that four of them were lying on one isotherm and four on one isochore. This allowed the measurement of the density and the temperature

derivatives of the structure factor. Five of the seven states coincide with those investigated in the experiment of [6].

Gaseous D_2 was liquefied in a cylindrical vanadium container with 10.6 mm internal diameter and 0.2 mm wall thickness using an He 'Orange'-type cryostat with a PID temperature controller. A second thermometer (Ge resistor), placed on top of the container, was used to measure the temperature T. The container was connected with a capillary to the gas handling circuit which included a calibrated transducer for the measurement of the pressure, and the number density n was calculated using the equation of state of Prydz [13]. The thermodynamic states are listed in table 1 and will be referred to by means of the number label in the first column of the table.

Table 1. Thermodynamic coordinates of the experiments. The estimated uncertainty in the temperature is $\Delta T = 0.1$ K. The equation of state of Prydz [13] has been used to determine the density and the isothermal compressibility, which give $S(0)$ via equation (24). For comparison, at the triple point $T = 18.71$ K and the density of the liquid phase is $n = 25.99$ nm^{-3}. The melting temperature varies from 18.76 K at the lowest pressure (state 1) to 19.72 K at the highest pressure (states 4 and 5).

State	T (K)	n (nm^{-3})	$S(0)$
1	20.6	25.48 ± 0.02	0.068
2	20.7	25.85 ± 0.03	0.066
3	22.0	25.45 ± 0.01	0.074
4	20.6	26.32 ± 0.02	0.062
5	23.3	25.52 ± 0.01	0.075
6	20.7	26.06 ± 0.01	0.063
7	22.7	25.54 ± 0.06	0.075

The scattered intensity has also been measured with the container filled with ^{3}He in such a quantity as to reproduce the same attenuation in the sample as present in the D_2 measurements. This technique, which is based on the extremely high absorption cross-section of ^{3}He, that makes it a practically perfect thermal neutron absorber, is an alternative to the more common use of empty cell measurements combined with the calculation of the Paalman and Pings coefficients [14], but it can allow a more accurate subtraction of the container scattering.

The total counting time for each sample has been divided into sub-runs of one hour each for the purpose of checking the stability of the system. The statistical error for one detector cell and each sub-run was $\approx 0.5\%$ and $\approx 1\%$ for D_2 and ^{3}He respectively, and for each sample at least eight sub-runs were performed. The count rates in the various sub-runs for the same sample, after normalization to the monitor counts, differed by an amount slightly larger than what was expected on the basis of the counting statistics, revealing that we have reached the limit of reproducibility of the experimental conditions. Therefore the normalized count rate in each cell has been averaged over all sub-runs relative to the same sample, and we have taken for the error the standard deviation of this average, which turns out to be $\approx 0.2\%$ for D_2 and $\approx 0.3\%$ for ^{3}He. The relative efficiency of the various cells, obtained from a calibration run, has also been taken into account.

4. Data treatment

In order to extract the structure factor from a neutron diffraction experiment, a number of corrections must be performed for various effects that influence the scattering signal. The

data have been first corrected for the detector dead time, which reduces the signal by a factor $1-\tau R$, where R is the measured count rate on the whole detector and the dead time is $\tau = 5\ \mu s$. The subtraction of background and container scattering is then performed by taking the difference between the resulting spectra I_{D_2} and I_{He}. In figure 1 it is shown that the use of the ^{3}He technique effectively removes from the diffraction pattern the Bragg peaks mainly due to the aluminium walls of the cryostat.

With respect to the ideal situation where the scattered neutrons originate from a point sample and impinge on a point detector, the finite size of the scattering volume and of the detector elements introduces deviations which increase with decreasing θ. For a given nominal scattering angle, there is actually a distribution of θ values that is not symmetric at low angle and its mean value differs slightly from the nominal one. The angular scale has been therefore corrected for this discrepancy. Also, the width of the θ -distribution contributes to the Q resolution with $\Delta Q/Q = \frac{1}{2}\tan^{-1}(\theta/2)\Delta\theta$, but it has been checked that the corresponding broadening of the main peak of the diffraction pattern is negligible.

4.1. Attenuation and multiple scattering

The intensity measured when the container is filled with D_2 and with ^{3}He is given by

$$I_{D_2} = I_{D_2}^{(1)} + I_{D_2}^{(m)} + I_b \tag{5}$$

and

$$I_{He} = I_{He}^{(1)} + I_{He}^{(m)} + I_b. \tag{6}$$

Here the superscripts (1) and (m) refer to the primary and the multiple scattering, respectively, which occur and are attenuated in the sample and in the container, while the background signal I_b is due to neutrons that partly go through the sample and/or the container and partly travel outside the scattering volume.

With the notation of the Paalman and Pings [14] attenuation coefficients,

$$I_{D_2}^{(1)} = A_{s,sc} I_s^{(1)} + A_{c,sc} I_c^{(1)} \tag{7}$$

$$I_{He}^{(1)} = A_{c,sc} I_c^{(1)} \tag{8}$$

where $I_s^{(1)}$ and $I_c^{(1)}$ are the scattering from sample alone and from container alone, corrected for the attenuation. In (8) we have assumed that there is no scattering from ^{3}He. The first subscript in the A denotes the region where the neutron is scattered; the second refers to the volume where the attenuation takes place. Combining equations (5) to (8), the single scattering from the sample alone, using the ^{3}He technique, is obtained as

$$I_s^{(1)} = \frac{1}{A_{s,sc}}\left[(I_{D_2} - I_{He}) - (I_{D_2}^{(m)} - I_{He}^{(m)})\right]. \tag{9}$$

$A_{s,sc}$ has been evaluated as a function of Q for the various densities of deuterium, using an algorithm based on the Soper and Egelstaff [15] method, which correctly accounts for the presence of the container.

With a similar program the multiple scattering has been evaluated in the approximation of isotropic single scattering, obtaining for all runs a Q dependence of the form $I^{(m)} = a + bQ^2$ where the quadratic term is very small (it amounts at most to 0.7% of $I^{(m)}$ for D_2 and 2.4% for ^{3}He) and the coefficients a and b are linear functions of the density. The ratio of multiple to total scattering, in the isotropic scattering approximation and neglecting the weak Q dependence by taking an average value, varies between 21.3% and 21.8% for the D_2 measurements and equals 1.8% for the ^{3}He runs. From this, the multiple scattering in

(9) can be estimated to contribute ≈25% of the total intensity. In section 4.4 an independent estimation of multiple scattering will be obtained with a different procedure and compared with the present result.

4.2. Inelastic scattering

The measured intensity, after correction for attenuation and multiple scattering, is

$$I(\theta) = \Phi N \Delta\Omega \int_{\substack{-\infty \\ \theta=const}}^{E_0/\hbar} d\omega\, \varepsilon(k_1) \frac{d^2\sigma}{d\Omega\, d\omega}(\theta, \omega) \tag{10}$$

where Φ is the incident neutron flux, ε is the detector efficiency, which depends on the speed of the scattered neutron, and $\Delta\Omega$ is the solid angle subtended by the detector element at the scattering angle θ. $I(\theta)$ is not proportional to the differential cross-section

$$\frac{d\sigma}{d\Omega}(\theta) = \int_{\substack{-\infty \\ \theta=const}}^{E_0/\hbar} d\omega \frac{d^2\sigma}{d\Omega\, d\omega}(\theta, \omega). \tag{11}$$

The effect of inelastic scattering is easily understood by noting that the integrals in (10) and in (4) are in general different. In contrast, if the scattering were a purely elastic process ($\omega = 0$) with $Q = Q_{el} = 2k_0 \sin(\theta/2)$, the intensity would be

$$I_{el}(\theta) = \Phi N \Delta\Omega\, \varepsilon(k_0) \frac{d\sigma}{d\Omega}(\theta) \tag{12}$$

while in (4) one could put $d^2\sigma/d\Omega d\omega = (d\sigma/d\Omega)\delta(\omega)$ and obtain (the two conditions $\theta = \text{constant}$ and $Q = \text{constant} = Q_{el}$ being now equivalent)

$$\tilde{S}(Q) = \tilde{S}(Q_{el}) = \frac{d\sigma}{d\Omega}(\theta) = v(Q_{el}) + u(Q_{el})[S(Q_{el}) - 1]. \tag{13}$$

Thus, $S(Q_{el})$ is directly related to $I_{el}(\theta)$ via (12) and (13). Using (10) one has

$$I(\theta) = I_{el}(\theta) + \Phi N \Delta\Omega\, \varepsilon(k_0) \left[\int_{\substack{-\infty \\ \theta=const}}^{E_0/\hbar} \frac{\varepsilon(k_1)}{\varepsilon(k_0)} \frac{k_1}{k_0} \tilde{S}(Q, \omega)\, d\omega - \tilde{S}(Q_{el}) \right]. \tag{14}$$

Denoting by $P(Q_{el})$ the bracket in (14), the connection between the measured intensity and the structural quantity of interest can then be written as

$$I(\theta) = I_{el}(\theta) + CP(Q_{el}) = C\{v(Q_{el}) + u(Q_{el})[S(Q_{el}) - 1] + P(Q_{el})\} \tag{15}$$

where $C = \Phi N \Delta\Omega\, \varepsilon(k_0)$ is a normalization constant to be determined and $I(\theta)$ is to be identified with the experimental quantity of (9). In the following we will write Q instead of Q_{el} for ease of notation. $P(Q)$ appears to play the role of an additive correction that accounts for the presence of inelastic scattering. Since the dynamics of the system is unknown, $P(Q)$ can be calculated for a model system, assuming that the result is a good approximation to the real case. The efficiency of the 7C2 detector is given by $\varepsilon(k) = 1 - \exp(-f/k)$ where f is a characteristic constant of the detector with the value $f = 17.65\ \text{nm}^{-1}$.

4.3. The diatomic ideal gas model

For a sample composed of non-interacting rotating harmonic oscillators (i.e. a diatomic ideal gas), one obtains with some calculations [10, 11]

$$\tilde{S}(Q, \omega) = u(Q) S_d(Q, \omega) + \sum_{J_0 J_0 \nu_1 \ell} a(Q; J_0, J_1, \nu_1, \ell) S_s(Q, \omega - \omega_{J_0 J_0} - \nu_1 \omega_v) \tag{16}$$

where J_0 and J_1 are rotational quantum numbers, ν_1 is a vibrational quantum number, ℓ is an integer satisfying the condition, $|J_0 - J_1| \leqslant \ell \leqslant J_0 + J_1$, $\omega_{J_0J_1}$ is the frequency of the $J_0 \rightarrow J_1$ transition, ω_v is the frequency of the molecular vibration, and the expression of the coefficients a is given in [11]. Equation (16) is derived with the hypothesis that only the ground vibrational state is thermally populated (for D_2, $\hbar\omega_v/k_B = 4307$ K, where k_B is the Boltzmann constant). The intermolecular cross-section is given by [11]

$$u(Q) = b_{coh}^2 \left| \int_{-1}^{1} dx \exp(i\beta x) \exp\left(-\frac{1}{2}\alpha^2 x^2\right) \right|^2 \tag{17}$$

while $v(Q)$ equals the infinite sum of the coefficients a and turns out to be [11]

$$v(Q) = 2(b_{coh}^2 + B_{inc}^2) + (b_{coh}^2 - \eta b_{inc}^2) \int_{-1}^{1} dx \exp(2i\beta x) \exp(-2\alpha^2 x^2) \tag{18}$$

where b_{coh} and b_{inc} are the bound atom coherent and incoherent scattering lengths of the nuclei, $\alpha = Q(\hbar/2M\omega_v)^{1/2}$, M is the molecular mass, $\beta = Qr_e/2$, r_e is the equilibrium internuclear distance, $\eta = (1 - c/c_n)/2I$, c and c_n are the actual ortho-species concentration and its normal (i.e. $T = \infty$) value, and I is the spin of the nucleus. For the centre of mass dynamics, the ideal gas formulae hold:

$$S_d(Q, \omega) = 0 \tag{19}$$

$$S_s(Q, \omega) = \frac{1}{Q}\left(\frac{M}{2\pi k_B T}\right)^{1/2} \exp\left[-\frac{M}{2k_B T Q^2}\left(\omega - \frac{\hbar Q^2}{2M}\right)^2\right]. \tag{20}$$

Due to (19), $S(Q) = 1$ and $\tilde{S}(Q) = v(Q)$, which have to be substituted in (14) and (15). By numerically evaluating the integrals in (18) and (14), $P(Q)$ has been calculated with $J_0 = 0, 1$, which are the only rotational levels thermally populated at the temperature of the experiment. With the used incident energy $E_0 = 162.7$ meV the neutrons can excite rotational transitions with $J_1 = 0, 1, \ldots, 6$, but not the first vibrational state of D_2, therefore only $\nu_1 = 0$ has been considered. Moreover, because vanadium is a very poor catalyst for the para to ortho conversion of D_2, $c = c_n = \frac{2}{3}$ has been assumed.

The result of the calculation, which does not depend appreciably on the temperature, is shown in figure 2. The problem of the inelastic scattering correction, however, will be reconsidered in the next subsection.

4.4. Data normalization

The absolute normalization method applied to these experimental data is based on the well known fact that in molecular liquids the single-molecule correlations extend to larger Q values than the intermolecular ones do [16]. In D_2, in particular [6], the latter is confined within a Q range which is smaller than what is covered in the present experiment. Therefore, above a certain Q_{min}, equation (15) reduces to $I(\theta) \approx C[v(Q) + P(Q)]$ so that, after subtraction of the inelastic scattering effects, the data can be normalized with respect to the calculated intramolecular cross-section $v(Q)$. In this way an *internal calibration* is performed, which avoids the disadvantages implied in the need for carrying out an independent measurement on a standard reference incoherent scatterer.

This normalization could be obtained, in principle, by simply fitting $v(Q)$ to the high-Q data using C as the only free parameter. However, for this method to work properly, all the extra contributions to the high-Q intensity must have been correctly subtracted. In order to

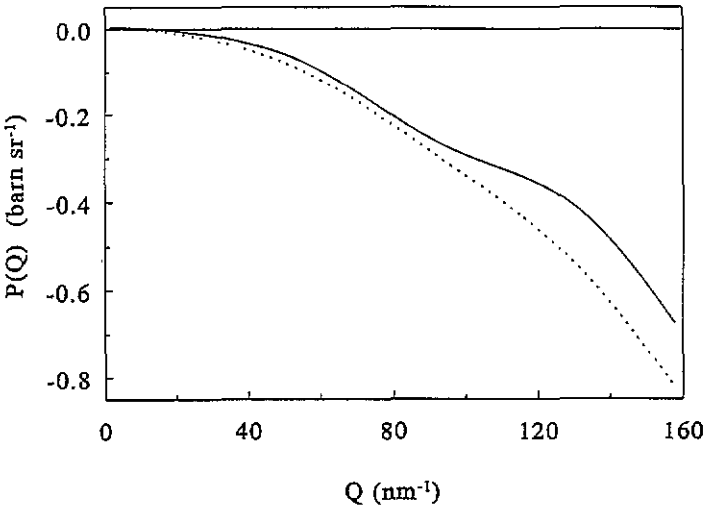

Figure 2. Inelastic correction: The solid line is $P(Q)$ calculated with the diatomic ideal gas model (see equation (14)); the dashed line is $P_{eff}(Q)$ obtained from the fit parameters via equation (22).

ensure this, an alternative procedure has been developed where a model function including these contributions is fitted to the data before the above-mentioned subtraction is performed.

As far as the inelastic correction is concerned, the fit function must allow for possible deviations from the $P(Q)$ calculated within the free-gas approximation. This shows (see figure 2) oscillations due to the molecular structure superimposed on the decreasing behaviour which is typical of a monatomic fluid and can be well described by a polynomial function of even powers of Q [17]. A more flexible fit function can be effectively obtained by including in it a linear combination of the calculated $P(Q)$ and a quadratic term. (Adding a Q^4 term does not modify appreciably the results). In this way the relative weight of the molecular modulation and of the centre of mass recoil effect can be adjusted and a better representation of the experimental data is obtained. Moreover, this model ensures that the low-Q behaviour approaches asymptotically the calculated $P(Q)$, giving a realistic description of the inelastic effects outside the fit range and avoiding the problem of an arbitrary extrapolation into the Q range where the information on the intermolecular structure is contained.

In a similar way, in order to account for a possible imperfection of the previous estimate of multiple scattering but retaining the information on its Q dependence obtained from the calculation, we have modelled this contribution with a quadratic term plus a constant one. The latter may also represent a residual constant background term, not completely subtracted. The fit function has been therefore taken in the form

$$\left(\frac{I_{D_2} - I_{He}}{A_{s,sc}}\right)_{fit}(Q) = A + BQ^2 + DP(Q) + C\left[\nu(Q) - 2(b_{coh}^2 + b_{inc}^2)\right] \tag{21}$$

where A, B, C, and D are free parameters of a linear fit and C is the desired normalization constant. In (21) BQ^2 represents the sum of the quadratic components of both the multiple scattering and the inelastic correction, and A contains the constant part of multiple scattering, a possible background contribution, and the asymptotic level of $\nu(Q)$ which is subtracted from the last term in order to reduce the correlation between the parameters. A similar representation of the diffraction intensity has been recently used in the analysis of neutron

data for other molecular liquids [18], although the contribution of molecular rotations could not be taken into account explicitly.

Table 2. Results of the fit. See text for the explanation of symbols. The last column reports the reduced χ^2 of the fits.

State	*A* (counts)	*B* (counts nm^2)	*C* (counts sr b^{-1})	*D* (counts sr b^{-1})	Reduced χ^2
1	58 745 ± 13	−0.738 ± 0.005	35 962 ± 72	17 332 ± 214	2.4
2	59 513 ± 14	−0.754 ± 0.005	36 500 ± 73	17 235 ± 215	2.2
3	58 551 ± 15	−0.751 ± 0.006	35 905 ± 79	16 725 ± 235	2.1
4	60 587 ± 14	−0.798 ± 0.005	37 042 ± 74	16 366 ± 221	1.8
5	58 402 ± 13	−0.764 ± 0.006	35 806 ± 71	16 081 ± 222	1.6
6	60 216 ± 19	−0.757 ± 0.007	36 843 ± 104	17 700 ± 300	1.4
7	58 954 ± 12	−0.749 ± 0.005	36 086 ± 67	17 000 ± 196	2.7

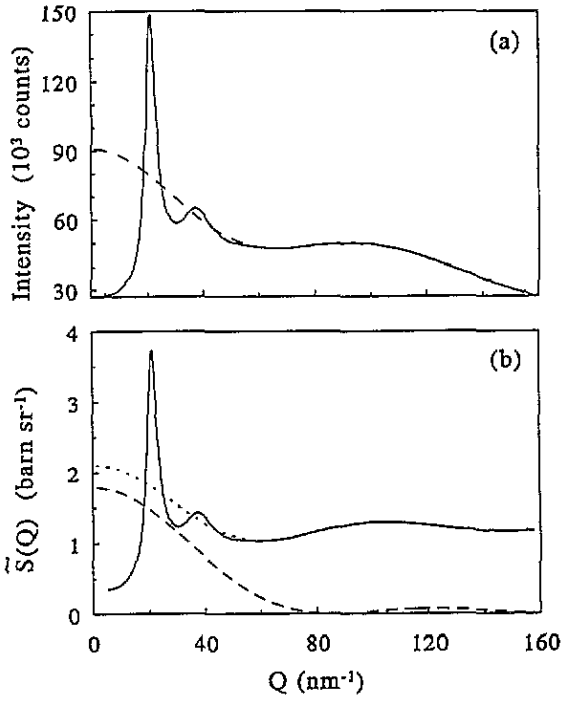

Figure 3. (a) Intensity for state 1 corrected for container scattering and attenuation: experimental data (solid line) and best fit of equation (21) to the single-molecule part (dashes); (b) $\bar{S}(Q)$ for state 1 (solid line), its single-molecule part $\nu(Q)$ (short dashes), and the intermolecular cross-section $u(Q)$ (long dashes).

The fit has been performed in the range $Q > Q_{min}$, where Q_{min} has been determined as the minimum value for which the fit parameters and the reduced χ^2 are independent of the fitting range. The quality of the fit is good, as shown in figure 3(a). In table 2 the fitted coefficients are reported for the various thermodynamic states. From the value of A, the multiple-scattering term in the right-hand side of (9) can be estimated, neglecting again the small quadratic term, as $(I^{(m)}_{D_2} - I^{(m)}_{He})/A_{s,sc} = A - 2C(b^2_{coh} + b^2_{inc})$ and turns out to be in

very good agreement with the result of the calculation of section 4.1 (for example, for state 1, the new estimate of the multiple-scattering fraction is 25.4%). This also indicates that no residual background is left in the data after the container subtraction performed with the ^{3}He technique, which is a clear confirmation of the usefulness of this correction method. Moreover, the Q^2 coefficient of multiple scattering can be estimated from the calculation of section 4.1 to be $B' \approx 0.02B$, so that the fitted quadratic term contributes nearly completely, together with the $DP(Q)$ term, to the determination of an effective inelastic correction

$$P_{eff}(Q) = \frac{1}{C}[(B - B')Q^2 + DP(Q)]. \tag{22}$$

The comparison of $P(Q)$ and $P_{eff}(Q)$, plotted in figure 2, shows that the inelastic effects are larger, but with weaker oscillations, than obtained from the ideal gas calculation, which however provides a rather good quantitative estimate.

Using the results of the fit to correct for multiple and inelastic scattering and to normalize the data, one obtains $\tilde{S}(Q)$, plotted in figure 3(b) together with $\nu(Q)$ and $u(Q)$. The centre of mass structure factor is finally obtained as

$$S(Q) - 1 = \frac{1}{Cu(Q)}\left[\left(\frac{I_{D_2} - I_{He}}{A_{s,sc}}\right) - \left(\frac{I_{D_2} - I_{He}}{A_{s,sc}}\right)_{fit}\right]. \tag{23}$$

In the investigated Q range, $u(Q)$ has one zero at $Q = Q_1 = 85.5$ nm^{-1}, around which the extraction of $S(Q)$ is impossible, but for D_2 the structural correlations are confined within the first 70 nm^{-1}. However, if the quantity in brackets in (23) differed appreciably from zero for $Q > Q_1$, thus revealing an inadequate fitting, the discrepancy would be amplified in the division by $u(Q)$ which in that region is always smaller than 0.07 b sr^{-1}. We have checked that this does not happen, which constitutes the most accurate proof of the validity of the fit procedure.

5. Results and comparison with TOF data

The experimental results for the centre of mass structure factor of D_2 are shown in figures 4 and 5. The statistical errors obtained from the regrouping of sub-runs (see section 3) have been propagated through the background and container subtraction, and have been used in the normalization weighted fit procedure. The statistical errors on the linear fit parameters can be obtained exactly, and the parameter covariances can also be calculated. The total experimental error $\Delta S(Q)/S(Q)$ is then obtained by propagating the errors through (23) and remains below the 1% level for $Q < 60$ nm^{-1}.

In figure 4 it is seen that the low-Q data may suggest an extrapolation to $Q = 0$ slightly below the thermodynamical limit (reported in table I)

$$\lim_{Q\to 0} S(Q) = S(0) = nk_BT\chi_T \tag{24}$$

where χ_T is the isothermal compressibility, while the high-Q asymptotic value

$$\lim_{Q\to\infty} S(Q) = 1 \tag{25}$$

is already reached at $Q = 70$ nm^{-1}.

In figure 5 the region of the main peak is enlarged to show the density and temperature variations. With increasing density along an isotherm, the peak height increases and the peak position is shifted to larger Q, while the increase of temperature along an isochore causes a lowering of the peak without shift.

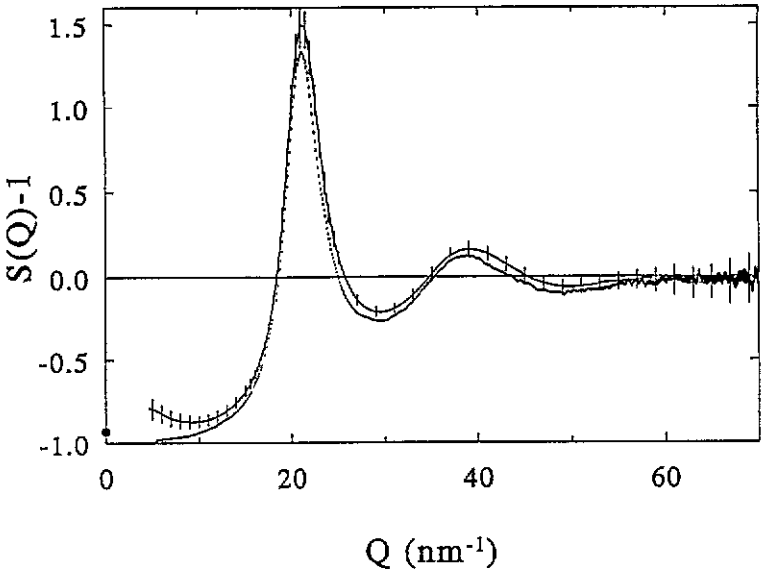

Figure 4. $S(Q) - 1$ for state 1 from this experiment (lower error bars) and from [6] (upper solid line with error bars). The dot at $Q = 0$ is obtained from thermodynamics.

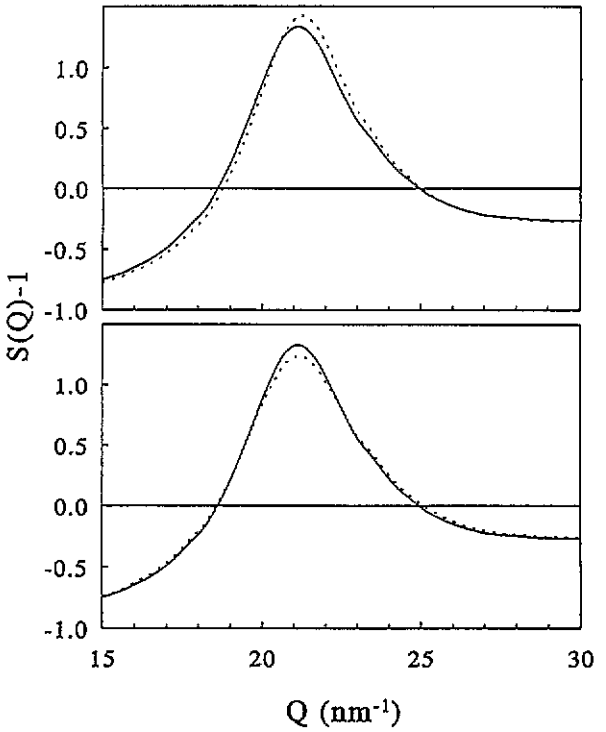

Figure 5. Top: $S(Q) - 1$ at different densities along the 20.7 K isotherm: solid line refers to state 1, dashed line to state 4. Bottom: $S(Q) - 1$ at different temperatures along the 25.5 nm^{-3} isochore: solid line refers to state 1, dashed line to state 5.

Figure 4 also reports the results of the TOF experiment of [6]. The comparison shows that a discrepancy is present, which is slightly greater than the experimental errors in [6]. These are much larger than in the present measurement because they take into account the variation of the diffraction pattern with the scattering angle due to some unexplained background contribution. Moreover, we have already recalled that at $Q < 10$ nm^{-1} the data of [6] are certainly affected by the presence of inelastic scattering which was not corrected for. In any case, the discrepancy between the two measurements appears clearly to be due to systematic effects, either present in the measured intensities or introduced by the inadequacy of some of the correction procedures, but not yet identified.

Strong support for this statement comes from the examination of the thermodynamic derivatives of $S(Q)$. We have determined $(\partial S(Q)/\partial n)_T$ for state 2 as the weighted average of the left and right derivatives obtained by numerical differentiation between states 1 and 2, and 2 and 4, while $(\partial S(Q)/\partial T)_n$ for state 3 has been derived analogously using the data for states 1, 3, and 5. The results, plotted in figure 6, are obtained with an experimental accuracy comparable with what has been so far reported in the literature only for monatomic fluids [19].

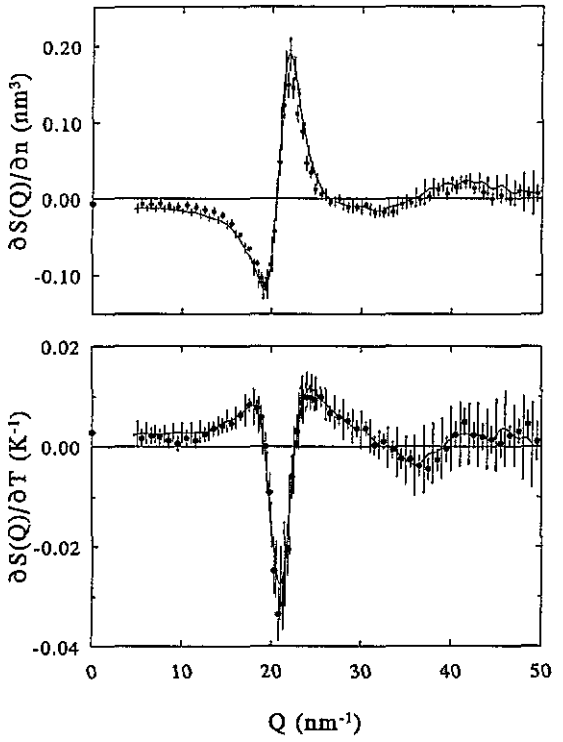

Figure 6. Thermodynamic derivatives of $S(Q)$ from this experiment (dots with error bars) and from [6] (solid line with error bars). Top: density derivative at constant temperature for state 2; bottom: temperature derivative at constant density for state 3. The dot at $Q = 0$ is obtained from thermodynamics.

In figure 6 the same quantities obtained from [6] are shown. The two measurements agree nearly everywhere with each other within the experimental errors, therefore better than for $S(Q)$, and only slight systematic differences can be discerned between 10 and 18 nm^{-1} and around 23 nm^{-1}. Moreover, for both derivatives, the low-Q data from both

experiments approach the thermodynamic value at $Q = 0$. It appears therefore that by taking the differences between the structure factors of thermodynamic states close to each other, most of the systematic errors that produce discrepancies in $S(Q)$ are effectively removed.

In [6] the density derivative of $S(Q)$ was compared with calculations based on various theoretical models of the triplet correlation function. Because of the agreement with the TOF data, the results there obtained apply to the present data as well and will not be repeated here.

6. Conclusions

We have performed a neutron diffraction experiment on liquid deuterium in the triple-point region in order to investigate the possibility of getting accurate data with a two-axis diffractometer on a low-mass molecular sample with a large amount of inelastic scattering, and we have carefully considered the problem of correcting for this effect.

We have measured the centre of mass structure factors at various thermodynamic states with a statistical uncertainty of the order of 1%, and from these the density and temperature derivatives of $S(Q)$ could be obtained with a great accuracy.

Having performed this experiment at the same thermodynamic states of a previous one [6], carried out on a time of flight diffractometer at a pulsed source, we have been able to compare the results of the two techniques, which are known to differ from each other especially when a significant amount of inelastic scattering affects the measured intensity. The comparison shows that the statistical accuracy obtainable with modern diffractometers is high enough to allow the detection of other sources of error, which appear to have the character of systematic effects. In fact, a difference method like the one required for the determination of the thermodynamic derivatives shows that most of these effects are present in the whole set of data taken in similar conditions and cancel out in a differential measurement.

We believe that the present determination of the structure factor of liquid D_2 is more accurate than that of [6], because each step of the data correction procedure has been performed under close control, and in some cases better techniques have been employed. For instance, the use of ^{3}He measurements, which allows a more accurate subtraction of container scattering, requires a monochromatic neutron beam and cannot be applied to TOF diffraction. The normalization of the data has been performed without recourse to a separate measurement, as done in [6]. The inelastic scattering correction, though very large at high Q (it amounts to $\approx$25% at $Q = 100$ nm^{-1}) has been accurately calculated with a realistic model and the information so obtained has been used to model the fit function with which the final subtraction was performed. As already mentioned, the same calculation would be practically impossible in the TOF case. Finally, the low-Q behaviour of the present data turns out to be in rather good agreement with thermodynamics.

The comparison with the TOF data shows, however, that the problem of obtaining very accurate diffraction data is not yet fully solved for all classes of sample. Work is in progress [20] to investigate possible reasons for the present discrepancies and efficient ways of reducing systematic errors to a level comparable with the available statistical accuracy.

Acknowledgments

We would like to thank J-P Ambroise for his skilful assistance during the experiment, and P Chieux and F Cilloco for useful discussions regarding various questions arising in the

course of the measurements and of the data analysis. We are also grateful to M Zoppi for a critical reading of the manuscript. One of us (EG) acknowledges the financial support of Istituto Nazionale di Fisica della Materia.

References

[1] Glyde H R and Svensson E C 1987 *Methods of Experimental Physics: Neutron Scattering* vol 23, ed K Sköld and D L Price (San Diego, CA: Academic) part B, ch 13 and references therein
[2] Zoppi M 1991 *Physica* B **168** 177
[3] Zoppi M, Magli R, Howells W S and Soper A K *Phys. Rev.* A **39** 4684
[4] Ishmaev S N, Sadikov I P, Chernyshov A A, Isakov S L, Vindryaevskii B A, Kobelev G V, Sukhoparov V A and Telepnev A S 1988 *Zh. Eksp. Teor. Fiz.* **94** 190 (Engl. Transl. *Sov. Phys.–JETP* **68** 190)
[5] Howe M A, McGreevy R L and Howells W S 1989 *J. Phys.: Condens. Matter* **1** 3433
[6] Zoppi M, Bafile U, Magli R and Soper A K 1993 *Phys. Rev.* E **48** 1000
[7] Egelstaff P A and Soper A K 1980 *Mol. Phys.* **40** 553, 569 and references therein
[8] van Kranendonk J 1983 *Solid Hydrogen* (New York: Plenum)
[9] Sears V F 1966 *Can. J. Phys.* **44** 1279
[10] Young J A and Koppel J U 1964 *Phys. Rev.* **135** A603
[11] Zoppi M 1993 *Physica* B **183** 235
[12] A complete report on this experimental work is in
Guarini E 1994 *Tesi di Laurea* Università di Firenze (in Italian)
[13] Prydz R 1967 *NBS Report* 9276
[14] Paalman H H and Pings C J 1962 *J. Appl. Phys.* **33** 2635
[15] Soper A K and Egelstaff P A 1980 *Nucl. Instrum. Methods* 178 415
[16] Powles J G 1973 *Adv. Phys.* **22** 1
[17] Yarnell J L, Katz M J, Wenzel R G and Koenig S H 1973 *Phys. Rev.* A **7** 2130
[18] Bellissent-Funel M-C, Bosio L and Teixeira J 1991 *J. Phys.: Condens. Matter* **3** 4065 and references therein
[19] Barocchi F, Chieux P, Magli R, Reatto L and Tau M 1993 *Phys. Rev. Lett.* **70** 947
Montfrooij W, de Graaf L A, van den Bosch P J, Soper A K and Howells W S 1991 *J. Phys.: Condens. Matter* **3** 4089
[20] Zoppi M, Bafile U, Magli R, Guarini E and Barocchi F 1995 to be published